CATEGORY 1

REGULATORY INFORMATION DISTRIBUTION SYSTEM (RIDS)

ACCESSION NBR:9810200203 DOC.DATE: 98/10/09 NOTARIZED: NO DOCKET #
FACIL:STN-50-528 Palo Verde Nuclear Station, Unit 1, Arizona Publi 05000528
STN-50-529 Palo Verde Nuclear Station, Unit 2, Arizona Publi 05000529
STN-50-530 Palo Verde Nuclear Station, Unit 3, Arizona Publi 05000530
AUTH.NAME AUTHOR AFFILIATION
LEVINE,J.M. Arizona Public Service Co. (formerly Arizona Nuclear Power
RECIP.NAME RECIPIENT AFFILIATION
MERSCHOFF,E.W. Region 4 (Post 820201)

SUBJECT: Forwards responses to questions numbered 5-9 from 980914 predecisional EC.Proprietary section from TR "SBLOCA Realistic Evaluation Model" encl.Proprietary info withheld, per 10CFR2.790(b)(1).

DISTRIBUTION CODE: IE91D COPIES RECEIVED:LTR 1 ENCL 1 SIZE: 10
TITLE: Dkt 50 Insp Rpt, etc.- Proprietary Enclosure

NOTES:STANDARDIZED PLANT 05000528
Standardized plant. 05000529
Standardized plant. 05000530

	RECIPIENT ID CODE/NAME	COPIES LTTR	COPIES ENCL	RECIPIENT ID CODE/NAME	COPIES LTTR	COPIES ENCL
	PD4-2 LA	1	0	PD4-2 PD	1	0
	FIELDS,M	1	0			
INTERNAL:	ACRS	2	0	FILE CENTER	1	1
	NRR/DRPM/PECB/B	1	1	NRR/DRPM/PERB	1	1
	NUDOCS-ABSTRACT	1	1	OE DIR	1	1
	OGC/HDS2	1	0	RES	1	0
	RES/DET/EIB	1	1	RGN4 FILE 01	1	1
EXTERNAL:	NOAC	1	ϕ w/out encl	NRC PDR	1	0

CATEGORY 1 DOCUMENT

NOTE TO ALL "RIDS" RECIPIENTS:
PLEASE HELP US TO REDUCE WASTE. TO HAVE YOUR NAME OR ORGANIZATION REMOVED FROM DISTRIBUTION LISTS OR REDUCE THE NUMBER OF COPIES RECEIVED BY YOU OR YOUR ORGANIZATION, CONTACT THE DOCUMENT CONTROL DESK (DCD) ON EXTENSION 415-2083

TOTAL NUMBER OF COPIES REQUIRED: LTTR 16 ENCL 7

IAY

APS

Palo Verde Nuclear Generating Station

James M. Levine
Senior Vice President
Nuclear

TEL (602)393-5300
FAX (602)393-6077

Mail Station 7602
P.O. Box 52034
Phoenix, AZ 85072-2034

102-04198-JML/AKK
October 9, 1998

Mr. E. W. Merschoff
Regional Administrator, Region IV
U. S. Nuclear Regulatory Commission
611 Ryan Plaza Drive, Suite 400
Arlington, TX 76011-8064

Dear Mr. Merschoff:

Reference: NRC letter dated September 23, 1998, from Arthur T. Howell, Director, Division of Reactor Safety, to James M. Levine, Senior Vice President, Nuclear

Subject: Palo Verde Nuclear Generating Station (PVNGS)
Units 1, 2, and 3
Response to NRC Questions, September 14, 1998
Pre-decisional Enforcement Conference

On September 28, 1998 Arizona Public Service Company (APS) letter 102-04186-JML/AKK was submitted responding to questions from the September 14, 1998 pre-decisional enforcement conference. In that letter responses to questions numbered 1 – 4 were submitted. Enclosed are the responses to questions numbered 5 – 9. Both letters respond to the NRC request of the Reference letter.

Attachment 2 to the Enclosure is a section from a topical report which contains information proprietary to ABB/CE. It is requested that this information be withheld from public disclosure pursuant to 10 CFR 2.790 (b)(1). An affidavit for this purpose was provided to the NRC with the original submittal of the full topical report via letter LD-93-141, S. A. Toelle (ABB) to Document Control Desk (NRC), "Submittal of Small Break LOCA Realistic Evaluation Model Topical Report", September 29, 1993.

No commitments are being made to the NRC in this letter. Should you have any questions, please contact Angela Krainik at (602) 393-5421.

Sincerely,

James M. Levine

Enclosure

JML/AKK/rlh

T. F. Stetka
P. H. Harrell
M. B. Fields
J. H. Moorman

1
1
FEPI

Change LTR to N.L
PUR 1 w/o prop

Enclosure

Response to NRC Questions, September 14, 1998 Pre-decisional Enforcement Conference

5.A) Provide an explanation of how the HPSI Check Valve as-found conditions were factored into the Maintenance Rule decisions.

U1, U2, and U3 HPSI systems were put into a(1) on August 18, 1998, in Expert Panel Meeting #170 due to a repetitive functional failure identified on HPSI check valve (1PSIAV 0404) after performing corrective maintenance. On September 24, the HPSI system unavailability was reviewed during Maintenance Rule Expert Panel Meeting # 174. The Expert Panel adopted the position that the HPSI check valve failure would impact unavailability on the redundant HPSI train when the HPSI pump on the same train as the failed check valve was taken out of service and was unable to start. The reverse flow could only exist if two conditions existed simultaneously. First, the check valve had to be failed. Second, the HPSI pump on the same train as the failed check valve was unavailable. If both pumps were available, the back flow would not occur. See Attachment 1.

The following unavailability times have been added to the redundant HPSI trains, after reviewing clearances, Electrical/Mechanical/I & C work, and outages that affect the HPSI pump availability.

Failure of 1PSIAV404 has added the additional unavailability time of 45.45 hours to Unit 1 HPSI Train B.
Failure of 2PSIBV405 has added the additional unavailability time of 64.48 hours to Unit 2 HPSI Train A.

5.B) Provide an explanation of how the HPSI Check Valve as-found conditions were factored into the INPO Plant Safety System performance indicator, (SSPI)

The SSPI "Fault Exposure Unavailability Hours" will be reported using the same method as reporting for the Maintenance Rule decision addressed in 5A. Currently, as EPIX database is structured, PVNGS is not able to report multi-unavailabilities for a single train. This will be communicated to INPO.

6. **Address dose consequences of the failed HPSI check valves following a Recirculation Actuation Signal if the HPSI injection valves are open (i.e., radioactive water would be re-circulated to the RWT through the mini-flow recirculation lines).**

Upon receipt of the Recirculation Actuation Signal (RAS), the PVNGS design provides for automatic closure of the Emergency Core Cooling System (ECCS) and Containment Spray (CS) pump RWT recirculation line (miniflow) isolation valves. These valves are SIA-UV-666 / SIB-UV-667, SIA-UV-669 / SIB-UV-668, and SIA-UV-664 / SIB-UV-665 for the HPSI, LPSI, and CS systems, respectively. The PVNGS design also includes automatic closure on a RAS of the combined recirculation line isolation valves SIA-UV-660 and SIB-UV-659 to ensure isolation of the RWT from the sump fluid.

Failure of these miniflow isolation valves to close could only exist in the event of a single failure of a diesel generator, concurrent with loss of off-site power and assuming the injection header isolation valves have opened. In this case the failed train (motor operated) miniflow isolation valves will not actuate and will remain open at the point of RAS. However, the combined recirculation line isolation valves are solenoid operated and receive DC battery power which will ensure that the valves will actuate on a RAS to isolate the RWT from the containment sump fluid. Further, these solenoid operated valves are fail-closed which ensures that a complete power failure of a train again results in isolation of the RWT from the sump. Consequently, there was no increase in the dose consequences as a result of the failed HPSI discharge check valves.

7. **Determine the consequences of RWT check valve leakage during the period when 2CHB-305 and 2SIB-405 were degraded.**

An evaluation has been prepared which documents the effect of the failed HPSI discharge isolation check valve 2SIB-V-405 concurrent with the degraded condition found for the RWT discharge isolation check valve 2CHB-V-305. This evaluation is based on the assumption of a single failure of the train B diesel generator, concurrent with loss of off-site power, and the HPSI header isolation motor-operated valves open. For this condition, elevated ESF pump suction line pressure would have occurred following a RAS. Leakage to the RWT would have increased with a proportional increase in dose consequences, relative to the current PVNGS LOCA dose analysis. However, the increase has been demonstrated to be small and the resultant doses well within the current PVNGS licensing basis.

The analysis demonstrates that leakage past the HPSI discharge isolation check. (2SIB-V-405) results in an increased pressure in the ECCS pump common suction header. The degraded HPSI check valve results in a maximum suction header pressure of approximately 228 psig, relative to the normal pressure of approximately 40 psig resulting from the static head of the water in the

containment sump. Thus, the pressure differential across the RWT discharge isolation check valve is increased which facilitates a corresponding increase in the leak rate back to the RWT.

During the period in which both valves were in a degraded condition, a leak rate and corresponding test pressure differential across the RWT discharge isolation check valve was obtained during surveillance testing. The excessive leak rate resulted in disassembly and inspection of the RWT discharge isolation check valve.

The inspection of the RWT discharge isolation check valve provided evidence that the check valve disk was misaligned due to excessive clearance between the disk stud to hinge arm connector As a result, the check valve disc was angled in the seat and may be considered effectively a flow orifice whereby the flow through the component, or in this case the leakage, is proportional to the pressure differential across the check valve. Hence, as stated above, the higher ECCS common suction header pressure would increase the leak rate to the RWT.

The analyses determine an effective loss coefficient for the RWT discharge isolation check valve based on the surveillance test data. Given the loss coefficient, the leak rate has been established assuming the maximum ECCS pump suction header pressure and the minimum RWT water level. The resultant leak rate, combined with the recorded leak rate through the opposite train (2CHA-V-306) conservatively results in a leak rate of 60 gpm. This is an approximate increase of 25% relative to the check valve surveillance test criteria and LOCA dose analysis assumption of 43 gpm.

The increased leak rate to the RWT results in a proportional increase in the total LOCA dose attributed to the RWT source term. The dose results were reviewed and concluded that the limiting dose, in terms of available margin, is the low population zone (LPZ) thyroid dose at 30 days. Factoring in an increase in RWT leak rate from 43 gpm to 60 gpm, the contribution from this leak path results in an approximate increase in the LPZ thyroid dose of 2%. The resultant dose is still well below the licensing basis value of 217.5R documented within the SER to Technical Specification Amendments 111, 103 and 83.

8.A Provide an explanation of the as-found small-break loss-of-coolant accident analysis, including the codes used. Address the compatibility and appropriateness of the codes. Specifically, describe the swelling and rupture models used, comparison with NUREG 630 Models, the data upon which the model was based and the results of the review. Please explain your use of the REM model when best estimate NRC models are available and are based on prototypical data.

The degraded HPSI flow analysis consisted of two parts: (1) blowdown hydraulics analysis using the CEFLASH-4AS computer code and (2) hot rod heatup analysis using the PARCH computer code.

(1)The blowdown hydraulic portion of the analysis was performed with ABB's NRC-accepted SBLOCA evaluation model version of the CEFLASH-4AS computer code. With one exception it was performed in compliance with the requirements of ABB's NRC-accepted SBLOCA evaluation model. The one exception is that the decay heat model inputs to CEFLASH-4AS were revised to approximate the 1979 ANS decay heat standard with +2σ uncertainty. In comparison, the ABB SBLOCA evaluation model uses 120% of the 1971 ANS decay heat standard as required by Appendix K to 10 CFR 50.

(2)The hot rod heatup portion of the analysis was performed with ABB's SBLOCA Realistic Evaluation Model (REM) version of the PARCH computer code. It used the same decay heat model as used in the blowdown hydraulics analysis. The REM version of the PARCH code (herein referred to as PARCH/REM) is a modified version of ABB's NRC-accepted SBLOCA evaluation model version of the PARCH code (herein called PARCH/EM). The following are the major differences between PARCH/REM and PARCH/EM.

Forced Convection Model - A forced convection model was added to PARCH/REM. PARCH/EM only analyzes the pool boiling portion of the SBLOCA transient. The PARCH/REM forced convection model was not used in the PVNGS SBLOCA analysis of the degraded HPSI flow. The forced convection portion of the transient was calculated by the STRIKIN-II code in ABB's NRC-accepted SBLOCA evaluation model

Decay Heat Model - PARCH/REM uses the 1979 ANS decay heat standard with +2σ uncertainty. As described above, the PVNGS SBLOCA analysis of the degraded HPSI flow used a decay heat curve that approximates the 1979 ANS decay heat standard with +2σ uncertainty.

Cladding Oxidation Model - PARCH/REM uses the correlations of Cathcart-Pawel for high temperature oxidation and Biederman for low temperature oxidation.

Cladding Swelling and Rupture Model - PARCH/REM uses a strain-to-failure model for determining cladding rupture.

The NUREG-0630 cladding swelling and rupture models were not used in the degraded High Pressure Safety Injection (HPSI) flow analysis. The analysis used the ABB small break LOCA (SBLOCA) Realistic Evaluation Model (REM) cladding swelling and rupture models. The REM cladding swelling and rupture models are described in Section 2.16 of Volume I of the ABB SBLOCA REM topical report (Reference 1). A copy of this section of the proprietary topical report is provided as Attachment 2.

The ABB SBLOCA REM topical report was submitted to the NRC for review in 1993 (Reference 2). However, it has not been reviewed by the NRC and ABB has recently notified the NRC of its decision to withdraw it from consideration for review and approval (Reference 3). Reference 4, which is an earlier version of the ABB SBLOCA REM topical report, was reviewed by the NRC and its contractor, Idaho National Engineering Labs (INEL). In response to the Requests for Additional Information (RAIs) that resulted from the review, Reference 4 was retracted by ABB and subsequently rewritten to incorporate the responses to the RAIs. The rewritten topical report was then resubmitted as Reference 1. The cladding swelling and rupture models described in Reference 1 are essentially unchanged from the Reference 4 models which were reviewed by NRC and INEL. However, additional descriptive material has been included in Section 2.16 of Reference 1 in a response to the RAIs related to the cladding swelling and rupture models.

Section 2.16 of Reference 1 describes in detail the cladding swelling and rupture models. The description includes an assessment of the models versus test data and a discussion of the applicability of the models to SBLOCA analyses. The material in Section 2.16 provides the basis for judging the acceptability of the ABB SBLOCA REM cladding swelling and rupture models.

In summary, there are three major differences between the model used in the PVNGS SBLOCA analysis of the degraded HPSI flow and the NRC-accepted ABB SBLOCA evaluation model: the decay heat curve, the cladding oxidation model, and the cladding swelling and rupture model. The methodology used in the SBLOCA analysis performed for the safety assessment of the degraded HPSI flow condition, including the ABB SBLOCA REM cladding swelling and rupture model, is appropriate for the analysis of degraded HPSI flow rate conditions that could have resulted from a back leakage through the failed check valves.

8.B The Cathcart-Pawel (C-P) oxidation model was apparently used. Explain which C-P model, was used and how it accounts for pressure enhancement due to RCS pressure

The degraded HPSI flow analysis used the ABB SBLOCA REM cladding oxidation model. The ABB SBLOCA REM cladding oxidation model is described in Section 2.15 of Volume 1 of the ABB SBLOCA REM topical report, Reference 1. The model uses the correlation's of Cathcart-Pawel (Reference 5) for high temperature oxidation and Biederman (Reference 6) for low temperature oxidation. The reaction rate constants for both correlations are taken at the upper 95% confidence

limit, that is, at roughly the two standard deviation upper bound to the normal best estimate values.

The oxidation model accounts for pressure enhancement due to RCS pressure. In particular, as described in Section 2.15.1.3 of Reference 1, the reaction rate correlations are modified by a pressure enhancement factor that is empirically derived from the data of Reference 7.

9. **Address the effect on Core Damage Frequency from the PRA perspective of the failed HPSI check valves.**

As documented in the LER, the PRA analysis was performed assuming that the degraded HPSI flow would have resulted in core damage. Since the deterministic analysis demonstrated that even with the degraded HPSI flow, safe shutdown could have been achieved and maintained, the increase in core damage frequency is negligible.

If the deterministic analysis is discounted, the PRA analysis of the risk associated with the degraded HPSI flow condition, assuming this condition leads to core damage, resulted in a core damage frequency increase of 3.3 E-05/year. This is approximately a 100% increase in baseline value. This analysis also includes the best estimate of HPSI unavailability due to maintenance activities.

References

1. CEN 420-P, Volume I, "Small Break LOCA Realistic Evaluation Model, Calculational Models," October 1993.
2. Letter LD-93-141, S.A. Toelle (ABB) to Document Control Desk (NRC), "Submittal of Small Break LOCA Realistic Evaluation Model Topical Report," September 29, 1993.
3. Letter LD-98-023, I.C. Rickard (ABB) to Document Control Desk (NRC), "Notification of Withdrawal of Topical Report CEN-420-P for Review," July 30, 1998.
4. CEN-373-P, Volume 1, "Realistic Small Break LOCA Evaluation Model – Volume 1 – Calculational Models," April 1988.
5. Cathcart, J.V. , and Pawel, R.E., et al, "Zirconium Metal-Water Oxidation Kinetics IV., Reaction Rate Studies," ORNL/1NUREG-17, August 1977.
6. Biederman, R. R., et al, "A Study of Zircaloy-4 Steam Oxidation Reaction Kinetics," EPRI NP-734, April 1978.
7. Pawel, Cathcart, Campbell, and Jury, "Zirconium Metal-Water Oxidation Kinetics vs. Oxidation of Zircaloy in High Pressure Steam," ORNL/NUREG-31, December 1977.

Attachment 1

HPSI Unavailability Graph

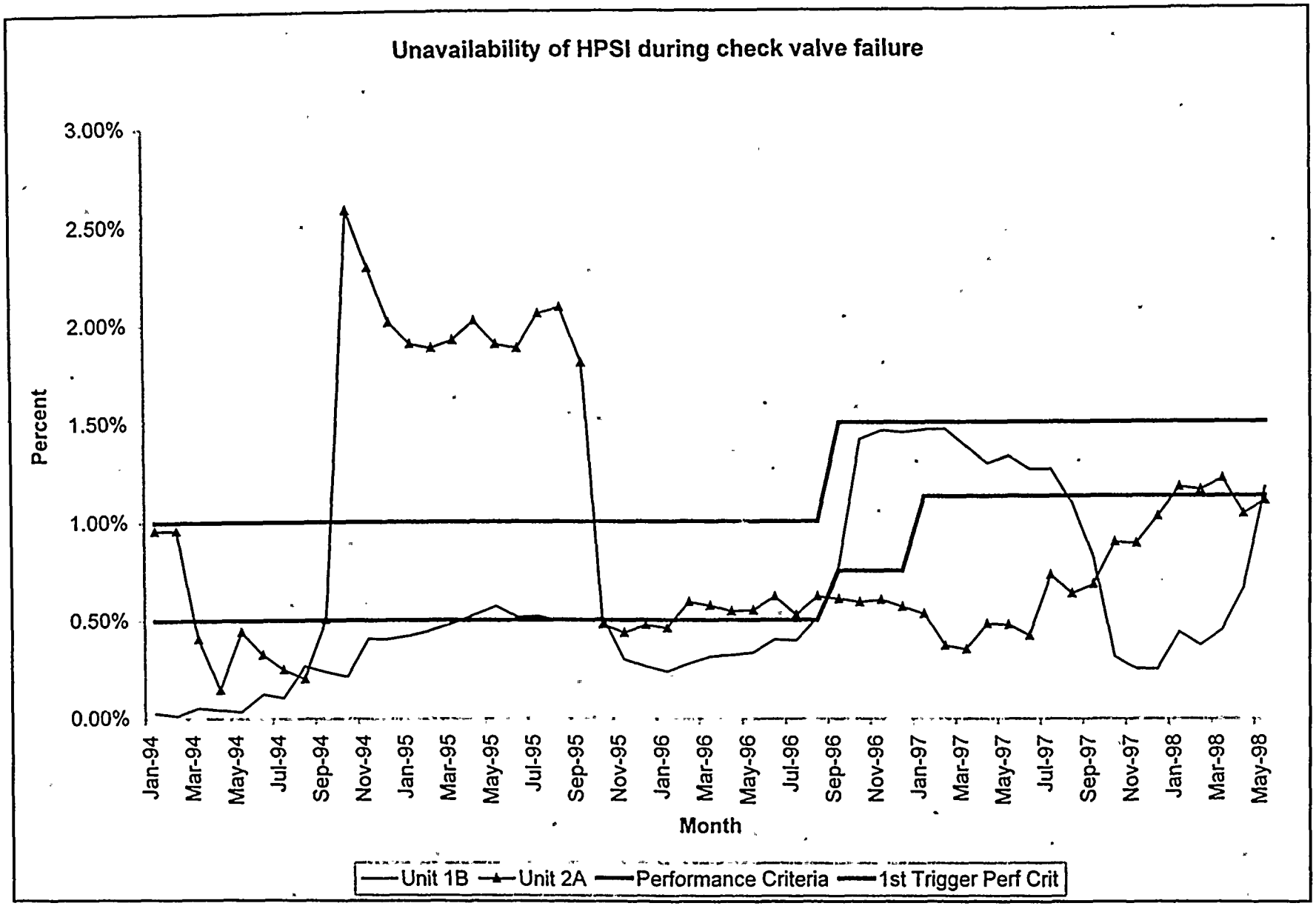
Unavailability of HPSI during check valve failure
3.00%
2.50%
2.00%
1.50%
1.00%
0.50%
0.00%
Percent
Jan-94
Mar-94
May-94
Jul-94
Sep-94
Nov-94
Jan-95
Mar-95
May-95
Jul-95
Sep-95
Nov-95
Jan-96
Mar-96
May-96
Jul-96
Sep-96
Nov-96
Jan-97
Mar-97
May-97
Jul-97
Sep-97
Nov-97
Jan-98
Mar-98
May-98
Month
Unit 1B
Unit 2A
Performance Criteria
1st Trigger Perf Crit

Attachment 2

Proprietary Information

Section 2.16 of CEN 420-P, Volume 1, Small Break LOCA Realistic Evaluation Model, Calculational Models, October 1993

~~3/30/1992~~ 2899

Copy No. 00035

CEN 420-P Volume I

SMALL BREAK LOCA REALISTIC EVALUATION MODEL

VOLUME I CALCULATIONAL MODELS

PREPARED
in cooperation with
THE C-E OWNERS GROUP

October, 1993

ANALYSIS DEVELOPMENT GROUP
FUEL ENGINEERING

ABB Combustion Engineering Nuclear Fuel

2.16 Cladding Swelling and Rupture Model

This section describes the models in PARCH/REM for analyzing cladding swelling and rupture. A mechanistic, cladding strain rate methodology along with a transient fuel rod internal pressure model is used to calculate cladding swelling and rupture.

2.16.1 Cladding Strain Model

The PARCH code for analyzing the hot rod cladding temperature calculates uniform plastic strain and checks for cladding rupture on each axial node at each time step. The model used in PARCH, referred to as CEMULTI, is a mechanistic, phenomenological method for predicting cladding deformation as a function of cladding temperature, heating rate, circumferential temperature gradient, differential pressure, and oxide thickness. The transient variation of cladding dimensions is used in PARCH to calculate the fuel rod gap conductance at each axial node. If rupture occurs, the rupture strain is used to expand the cladding surface area uniformly and reduce the cladding thickness. Also, cladding oxidation on the inside of the fuel rod at the rupture node is calculated.

In CEMULTI, the cladding is segmented into six circumferential zones to represent the effects of circumferential temperature gradient. Physically, one of these zones represents the hot spot and the remaining five represent one-half of the circumference of the cladding, extending from the hot spot to the diametrally opposed cold zone. The circumferential temperature gradient is defined as the hot spot temperature minus the average cladding temperature. PARCH calculates the average cladding temperature of the hot rod, and the circumferential temperature gradient is used to prescribe the temperature distribution needed to calculate cladding deformation. Based on out-of-pile experimental observations, this gradient is distributed to the hot, cold, and four intermediate circumferential zones, in the manner illustrated by Figure 2.16-1 and is assumed constant throughout the transient. The initial values of stress in all six zones are set equal to one another and are proportional to the average initial differential pressure across the cladding.

2.16.1.1 Correlation Description

The transient strain rate of each of the six zones is calculated from an empirical correlation which is a function of the burst stress (Equation 2.16-1). The burst stress is a function of the cladding temperature and oxide thickness of each zone. The total cladding strain attained during a PARCH time interval is obtained by integrating the effective strain rate over time. The effective strain rate is taken to be the arithmetic average of the individual zone strain rates, excluding the hot zone. The wall thickness strain is different for each zone; however, the diametral strain is assumed uniform. True stress in each zone is calculated using these values of wall thickness, diametral strain, gap pressure, and coolant channel pressure.

The burst stress (σ_{Bi}) and the transient strain rate ($\dot{\varepsilon}_i$) in each zone (i) are calculated from Equation (2.16-1). This expression is a C-E modified form of the KWU High Temperature Cladding Creep Model (Reference 2.16-3):

$$\dot{\varepsilon}_i = A\,\sigma_i^{n}\,EXP(-B/8.3144\,T_i)/(1-(\sigma_i/\sigma_{Bi})^2) \qquad (2.16\text{-}1)$$

where $n = 2.8$

$A = 500. + 1000.\,(R-5)/45$

$0. < R\ (°C/sec) < 50$

$$\sigma_{Bi} = A_1\,EXP(-B_1T_i)\,1.4\,(1-Z_{mi}) \qquad (2.16\text{-}2)$$

$Z_{mi} = -.32 + .32\,Z^{1/2}_{xm_i}$

if $T_i < 1115$

$A_1 = 4.86 \times 10^3$

$B_1 = 3.015 \times 10^{-3}$

$B = MAX(190000., BB) + 3000$

$BB = BA + 20.\,(T_i - 1173.16)$

$BA = 195940. - 450.\,(T_i - 1173.16)$

if $1115. < T_i < 1213.16$

$A_1 = 4.86 \times 10^3\,EXP(10.453)$

$B_1 = 1.239 \times 10^{-2}$

$B = MIN(BB, BA) + 3000$

if $T_i > 1213.16$

$A_1 = 4.86 \times 10^3$ EXP(-.92025)

$B_1 = 3.016 \times 10^{-3}$

$B = BA + 3000$

where

$\dot{\varepsilon}_i$ = strain rate of zone i (ft/ft/sec)

σ_i = engineering hoop stress of zone i (MPa)

T_i = cladding temperature of zone i (°K)

σ_{Bi} = burst stress of zone i (MPa)

R = heating rate (°C/sec)

Z_{xmi} = thickness of cladding oxide (μm)

n, A, B, A_1, B_1, Z_{mi}, BB, BA = correlation constants or parameters

In this strain-to-failure model, cladding failure is assumed to occur if the stress in the hot zone (or in the intermediate zone next to the hot zone) attains or exceeds the burst stress value at the corresponding zone temperature. Also, if the strain in the hot zone exceeds 300% (an arbitrarily large value), failure is assumed. The temperature of the hot zone at the time of failure is designated as the rupture temperature. The rupture strain is defined as the cumulative total strain generated in the integrated time up to rupture.

2.16.1.2 Correlation as Coded

The correlation in Equation (2.16-1) is coded in Subroutine CEMULTI as represented.

2.16.1.3 Correlation Assessment

CEMULTI calculations are assessed by comparing the predicted results against data from single rod burst tests in Figures 2.16-2 through 2.16-6. The data contains considerable scatter due to variations in local circumferential temperature gradients and heating rate. For example, the data in

Figure 2.16-2 ranges from 0.0 to 7.5°C circumferential temperature gradient and 0.8 to 1.6°C/sec heating rate. This variation produces a rupture strain scatter of ±20%. Therefore, the CEMULTI predictions are shown for the extremes of the parameter variation in order to bound the data. Figures 2.16-2 through 2.16-4 illustrate that CEMULTI predictions for rupture strain and rupture temperature adequately bound the data using the observed extremes in the parameter variation for GFK single rod burst tests, (Reference 2.16-4).

Figure 2.16-5 compares the CEMULTI prediction of rupture temperature versus differential pressure to the GFK data (Reference 2.16-4). The data scatter for rupture temperature is less pronounced than for rupture strain. Again, CEMULTI predictions are made for the extremes of the parameter variation. The comparison shows good agreement between CEMULTI predictions and the test data.

The CEMULTI model is used to predict the failure of C-E fuel rod cladding in Figure 2.16-6. Generally, these tests cover higher circumferential temperature gradients (10-60°C) which produce lower rupture strains. The CEMULTI comparisons using the extremes of the parameter variation for the data represented by solid symbols adequately bound this data set.

2.16.1.4 Applicability to Small Break LOCA Analysis

The PARCH/REM predictions were compared against test data for various heating rates (0.8 - 35 ^{0}C/Sec), differential pressures (10 - 130 Bars) and circumferential temperature gradients (0 - 60 ^{0}C). The code predictions match the data fairly well, as seen in Figures 2.16-1 - 2.16-6. The range of parameters considered is fairly wide and is expected to cover the values encountered in a SBLOCA. The correlation in Equation (2.16-1) is therefore, adequate for calculating cladding strain rates in a small break analysis.

2.16.2 Circumferential Temperature Gradient

In an actual assembly environment, the Circumferential Temperature Gradient (CTG) in a fuel rod may result from non uniformities in heat transfer both internal and external to fuel rod, due to numerous factors. Inside the fuel

rod, an eccentric pellet stack, pellet swelling and cracking during operation, etc. may cause the pellet to touch the cladding. This may lead to non uniform heat transfer and consequently, to circumferential temperature gradients. Outside the rod, inhomogeneous coolant flow conditions, rod to rod radiation and rod to rod mechanical interaction, etc. may lead to heat transfer non uniformities, resulting in circumferential temperature gradients. The relationship between these factors and the circumferential temperature gradient is complex and involves large uncertainties. Also, little experimental data in a multi rod environment is available to correlate the factors responsible for the heat transfer non-uniformities to CTG. Therefore, in the REM circumferential temperature gradient is modeled as a constant and is not calculated dynamically.

2.16.2.1 Model Assessment

The justification for use of a constant CTG value in the REM is based upon the data provided by the C-E SREPT test program conducted by KWU. These tests provide well characterized temperature, pressure, heating rate, and circumferential temperature gradient histories. The test conditions included internal electrical heating of single fuel rods enclosed by an unheated radiation shroud. Fuel pellets were simulated by specially designed alumina sleeves which surrounded the electrical heater and had the freedom to position eccentrically within the cladding. The off-center pellet was the only major source of circumferential temperature non-uniformity. Circumferential temperature gradients were determined from the data readings of three thermocouples placed around the cladding at the hot-spot elevation. A cosine profile was analytically fit to the three readings and the temperature gradient was expressed as the difference between the calculated peak of the cosine and the calculated mean.

The results form five of these single burst tests are shown in Figures 2.16-7 through 2.16-11. The nominal heating rates, initial differential pressures, rupture temperatures and rupture strains tested are given in Table 2.16-2. The Figures show cladding temperature readings and the inferred circumferential temperature gradient. The tests provide data on rupture

temperature and rupture strain for a range of typical reflood boundary conditions. These Figures show that during most of the transient (before rupture) the CTG does not vary significantly and therefore, in the REM the CTG is approximated as a constant.

2.16.2.2 Circumferential Temperature Gradient Sensitivity Study

Because of the complex nature of the dependence of CTG on the PCT, a PARCH/REM sensitivity study was performed to determine the effect of the circumferential temperature gradient on typical, REM transients. Circumferential temperature gradients typical of actual fuel rods have been measured in the NRU LOCA Simulation Test Program (References 2.16-5 and 2.16-6). Values range from 2 to 20°F. Actual measurement positions were not located in the regions of cladding deformation, so there is considerable uncertainty in these measurements. Out-of-pile tests with electrical heaters instead of nuclear fuel show even larger variations in circumferential temperature gradients, ranging from 1 to 100°F. Circumferential temperature gradients ranging from 5°F to 100°F were examined. A value of 15°F produced the highest cladding temperature. A value of 100°F resulted in only a 2°F lower cladding temperature, an 11 psia lower gap pressure, and a 10% lower gap conductance. The magnitude of the circumferential temperature gradient affects the cladding rupture strain and consequently the PCT. At low cladding temperatures, large circumferential temperature gradients produce more cladding swelling than low gradients because a larger portion of the cladding experiences higher temperatures for the same average temperature, hence more strain. At high cladding temperatures, large circumferential temperature gradients produce less cladding strain than low gradients because the swelling process is stopped by earlier cladding rupture. The magnitude of the rupture strain affects the balance between heat removal and heat generated and consequently, the cladding temperatures. Larger strains produce larger surface areas for convective cooling and decreased gap conductance between the fuel and the cladding, resulting in lower cladding temperatures. Because of these competing effects, the location of maximum cladding temperature usually occurs at elevations of unruptured cladding and depends on the depth and duration of core uncovery during the small break LOCA.

Since the sensitivity of peak cladding temperature to circumferential temperature gradient is not significant for these SBLOCA transients, the conservative value of 15 ^{0}F is used in the REM. This low value is consistent with effects observed for irradiated fuel rods where cladding collapse and fuel pellet fragmentation and relocation lead to more uniform circumferential cladding temperature distribution. This low value will assure the highest cladding temperatures for realistic plant analyses and also produce larger rupture strains for transients where ballooning and rupture occur.

2.16.3 Transient Fuel Rod Internal Pressure Model

The driving force for outward cladding deformation during a LOCA is the internal fuel rod pressur e minus the coolant pressure. Internal pressure during the LOCA is dependent on the fuel temperature and on the extent of cladding ballooning. The REM version of PARCH performs a transient calculation of the fuel rod internal pressure using the fuel rod pressure model from Reference 2.16-2. Internal pressure is initialized through plant parameter input at hot fuel rod dimensions.

During a LOCA transient, increasing fuel rod temperatures produce increasing internal pressure. As ballooning occurs, the local internal pressure decreases, thus allowing a gas flow to the region of deformation from a region of higher pressure, such as the fuel rod plenum. Cladding ballooning may be slowed by the resultant reduction in internal pressure. The PARCH model for gas pressure assumes that this gas flow instantly restores a quasi-steady, constant pressure to the fuel rod.

PARCH explicitly accounts for the effects of gas temperature and fuel rod volume by using the equation of state for an ideal gas at each time step:

$$P_{gap} = nR \left[\sum_{i} T_{gap,i}/V_i + \sum_{j=1}^{2} T_{pl,j} / V_{pl,j} \right] \qquad (2.16\text{-}3)$$

where nR is determined at initialization and held constant for the transient

$T_{gap,i}$ is the average between the cladding inside surface temperature and the fuel pellet outside surface temperature at node i

$T_{pl,j}$ is the plenum temperature

V_i is the gap volume at node i

$V_{pl,j}$ is the plenum gas volume

The temperature of the gas in the fuel rod plenums is taken to be that calculated for the coolant at the top and bottom elevations of the fuel rod.

2.16.3.1 Fuel Rod Internal Pressure Model as Coded

The rod internal pressure calculation is performed in Subroutine INTRPL using Equation (2.16-3). Equation (2.16-3) is coded as represented.

2.16.4 Cladding Deformation and Hot Rod Heatup Calculation.

2.16.4.1 General

As is described in Section 1.4 - Code Structure - PARCH/REM, the maximum cladding temperature in the core is determined by calculating the heatup of the "hot rod" with the PARCH/REM computer program. PARCH/REM basically uses a model consisting of a single fuel rod in a closed subchannel. Although subchannel flow blockage and subsequent flow diversion/redistribution caused by cladding deformation is not explicitly calculated by PARCH/REM, the effect of subchannel blockage is accounted for by reducing the subchannel steam flow (from boil-off and flashing) by a factor that in PARCH/REM is called "pin-to-box" ratio.

In the following sections it will be shown that the cladding temperatures calculated with PARCH/REM are slightly higher than cladding temperatures determined with an alternate model that explicitly calculates subchannel flow blockage and flow diversion/redistribution.

2.16.4.2 PARCH/REM Analysis

PARCH/REM represents a single fuel rod, surrounded by a closed subchannel, whereas in an actual assembly, a subchannel can freely communicate with the surrounding subchannels. One of the factors involved in the calculation of the subchannel steam flow is the pin-to-box ratio. The pin-to-box ratio is the ratio of the power of the highest-powered fuel rod (pin) in an fuel assembly (box) to the power of the average fuel rod in that assembly. The pin-to-box ratio is used in PARCH/REM to divide the single rod steam flow (which is calculated from boil-off and flashing) above the two-phase level in the entire subchannel channel and, thus, affects significantly the heat-up calculation of an uncovered fuel rod during the boil-off phase of a small break transient. The larger the ratio, the lower is the steam flow, and hence higher the PCT.

The input value for the pin-to-box ratio is a Limit Value (LV). As described in Section 3, the use of Limit Values is part of ABB-CE's "Limit Values Approach Plus Delta T Adders" uncertainty evaluation methodology. A Limit Value is that value within the range of a significant plant parameter that maximizes the peak cladding temperature. The Limit Value pin-to-box ratio is determined by first dividing the burnup cycle into small burnup intervals. The fuel rod with the highest peak linear heat generation rate (PLHGR) is then identified in each burnup interval. This identification results in a set of pin-to-box ratio/PLHGR data pairs for the fuel rods with the highest PLHGR. From these data pairs the highest pin-to-box ratio, corresponding to the maximum PLHGR allowed by the Technical Specifications is then selected for the Limit Value.

The peak linear heat generation rate is also a LV. Limit Value PLHGR is the maximum allowed by the Technical Specifications plus 1 kw/ft. The 1 kw/ft is

added to account for rods which may be lower in power than the highest powered rods identified in the burnup cycle intervals mentioned above and which may have higher pin-to-box ratios than the LV pin-to-box ratio.

This procedure assures that the PCT calculated with these Limit Values is higher than PCTs that could be calculated with any other actual fuel rod data pair.

2.16.4.3 Alternate Model

In order to quantify the impact of subchannel blockage and flow diversion on PCT, an alternate PARCH model was developed. In this alternate model the use of pin-to-box ratio to reduce the steam flow was replaced by including a time-dependent calculation of rod deformation and subchannel blockage as well as a calculation of flow diversion of the steam flow above the two-phase mixture level.

The subchannel blockage was dynamically calculated as a function of strain, using the blockage versus strain relationship provided in Appendix B of Reference 2.16-1 (NUREG-0630, page 111, Tabulation of Cladding Correlations, Slow-Ramp Correlations; also shown here in Table 2.16-1). The cladding strain model used in PARCH/REM is described in Section 2.16.1.

The flow diversion was calculated with the HCROSS computer program (Reference 2.16-7). HCROSS is a two-dimensional, steady state, adiabatic, single-phase flow code, developed by ABB-CE and used in LOCA licensing calculations. The code has been verified against flow diversion data from Battelle Northwest Labs (70% and 90% blocked subchannels tests, Reference 2.16-8), Westinghouse parallel blockage tests (Reference 2.16-9), and the Tapuca and Trocke subchannel tests (Reference 2.16-10) with an explicit flow diversion representation.

The PARCH code was modified to include HCROSS predicted minimum flow fraction in the blocked subchannel relative to flow in an unblocked subchannel as well as the flow recovery downstream of the blockage, as a function of the blockage

in the blocked subchannel. Although this alternate model accounts explicitly for subchannel blockage and flow diversion/redistribution, it still includes a number of conservatisms. These conservatisms are:

The HCROSS predicted axial flow fractions were applied to the hot rod steam flow (boil-off and flashing) at the two PARCH/REM coolant subchannel nodes near the top of the core corresponding to the fuel rod nodes with maximum deformation (throat) and the highest cladding temperature node just downstream of the throat. The flows in these PARCH/REM nodes were axially held constant at the HCROSS reduced values. No credit for the axial flow redistribution downstream of the blockage as predicted by HCROSS is taken.

HCROSS models two adjacent subchannels. One of which is partially blocked, the other totally unblocked to conservatively model the flow diversion from the hot channel. In reality the subchannels adjacent to the hot subchannel also have blockage. The case of a partially blocked hot subchannel with low blockages in the surrounding subchannels was not considered because this produces less flow diversion than the case where the surroundings are unblocked.

The HCROSS calculations were performed assuming maximum blockage of 71.5% (in the hot subchannel) prescribed in NUREG-0630, Reference 2.16-1.

A top peaked power shape is assumed in the analysis. This power shape allows longest time period of core uncovery to the highest powered nodes, resulting in maximum strain and flow diversion. Also, in PARCH/REM no credit is taken for the colder steam in adjacent subchannels mixing with the hot subchannel due to cross flow.

2.16.4.4 Results of the Sensitivity Study

Several PARCH/REM cases with different break sizes (.05 - .50 Ft^2) and two different plants (Calvert Cliffs and the Reference plant) with different fuel designs were analyzed with the alternate PARCH model. The Calvert Cliff plants are 2700 Mwt NSSS with a 14x14 fuel design. The Reference plant is a

3400 MWt NSSS with a 16x16 fuel design and has the combined characteristics of SONGS 2&3 and Waterford 2. The PCTs calculated by the alternate PARCH model with the code modifications for flow blockage and redistribution were compared to the LV PCTs case without flow blockage and redistribution. In the alternate PARCH model, all the parameters like PLHGR, pin internal pressure, gap conductance, axial power shape, etc. were used at their limit values except for the pin-to-box ratio which was set equal to 1. These PARCH cases with an explicit flow diversion representation resulted in PCTs lower than the Limit Value PCTs. For example the LV PCT for the limiting break (.14 Ft^2 , CLB) for the Calvert Cliffs is 1524 ^0F. The corresponding PCT calculated with the alternate PARCH model is 1497 ^0F, about 27 ^0F lower than the LV PCT. Similarly, for the Reference plant, the alternate PARCH model predicts PCT about 11 ^0F below the LV value for the limiting break (.05 Ft^2). In the Reference plant analysis, the clad did not strain enough to provide the maximum 71.5 % blockage. In order to maximize the effect of flow diversion due to blockage, the PARCH/REM coding for the Reference plant analysis was further modified to artificially force a maximum blockage of 71.5 %. The 11 ^0F PCT differential for the Reference plant analysis quoted above is based on this 71.5% artificially forced maximum blockage.

The above analysis which covers a wide range of break sizes and fuel types demonstrates that the limit value approach for calculating PCT on the hot rod includes enough margin to cover the effects of a very conservative representation of flow diversion due to blockage. The LV approach uses pin-to-box ratio to reduce the flow above the two-phase level to account for flow diversion. Therefore, even though in the LV approach the flow blockage and subsequent flow diversion/distribution caused by cladding deformation is not represented explicitly, the effect of flow diversion is adequately accounted for by using the LV pin-to-box ratio.

References for Section 2.16

2.16-1 NUREG-0630," Cladding Swelling and Rupture Models for LOCA Analysis," U.S.N.R.C.

2.16-2 CENPD-135, "STRIKIN-II, A Cylindrical Geometry Fuel Rod Heat Transfer Program", Combustion Engineering Proprietary Report, August 1974.

2.16-3 A Kunick, et. al., "High-Temperature Zircaloy Tube Deformation Model Considering Nonuniform Temperatures", ANS Trans. of ENC '79, 31, 342, Hamburg (Germany), May 1979.

2.16-4 Erbacher, F., et. al., "Burst Criterion of Zircaloy Fuel Claddings in a LOCA," KFK/PNS, ASTM Fifth International Conference on Zirconium in the Nuclear Industry, August 4-7, 1980, Boston, MA.

2.16-5 NUREG/CR-2509, "Materials Test-2 LOCA Simulation in the NRU Reactor," Battelle Pacific Northwest Laboratory, March 1982.

2.16-6 Handouts from Industry Review Meeting, "LOCA Simulation in NRU, Materials Test 3," Battelle Pacific Northwest Laboratory, Meeting held at Silver Spring, Maryland, February 3, 1982.

2.16-7 C-E ECCS Evaluation Model enclosure 1-P-A to LD-81-095, Dec. 1981

2.16-8 J.M. Creer, et al., "Effects of Sleeve Blockage on Axial Velocity and Intensity of Turbulence in a Unheated 7x7 Rod Bundle," "Battelle Pacific Northwest Laboratories Report, BNWL-1965, January, 1976.

2.16-9 H. Chelemer, et al.,"An Improved Thermal-Hydraulic Analysis Method for Rod Bundle Cores,"Nuclear Engineering an Design, Vol. 41, 1977, pages 219-229.

2.16-10 A.Tapucu and N. Troche, "Pressure Induced Diversion Cross-Flow for Rod Bundle Subchannels Interconnection Geometry," paper presented at the American Nuclear Society Annual Meeting, New York City, June 12-16, 1977.

Table 2.16-1
Flow Blockage Versus Strain
(Extracted From Reference 2.16-1, Appendix B)

Strain (%) ($\leq$10 ^{0}C/S)	Flow Blockage (%) ($\leq$10 ^{0}C/S)
10	6.5
11	7.0
13	8.4
20	13.8
45	33.5
67	52.5
82	65.8
89	71.0
90	71.5

Table 2.16-2
Experimental Conditions for C-E SREPT Burst Tests

Test No.	Initial Rod Pressure (Bars)	Heating Rate (^{o}C/Sec)	Rupture Temperature (^{o}C)	Rupture Strain (%)
19	90	10	798	42.3
20	90	10	798	26.6
31	70	2	779	21.8
49	90	2	768	32.5
50	70	2	768	40.2

Figure 2.16-1
Distribution of Circumferential Temperature Gradient
for Calculation of Cladding Swelling and Rupture

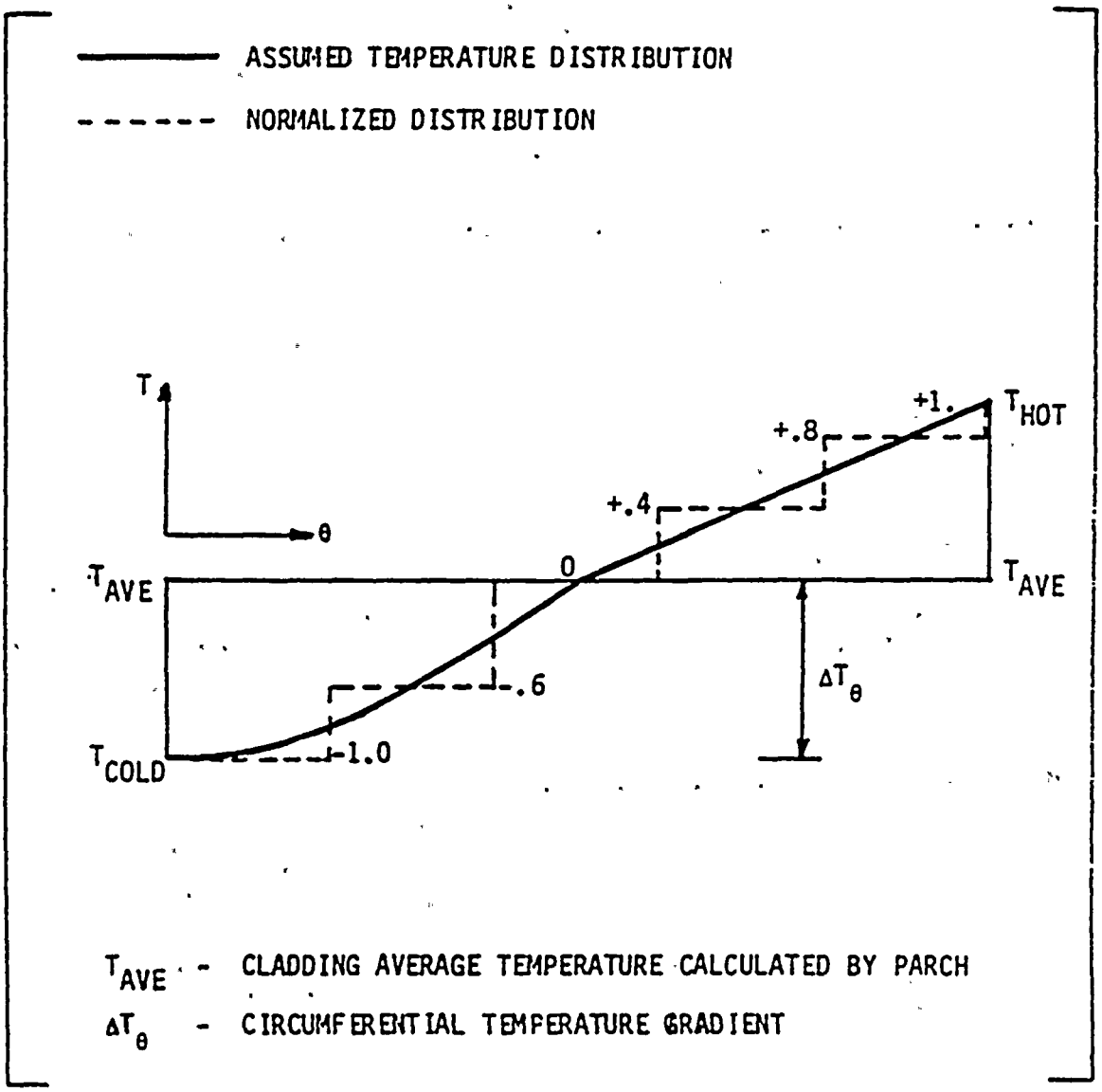

Figure 2.16-2
Comparison of CEMULTI to GFK Data
Rupture Strain Vs. Rupture Temperature

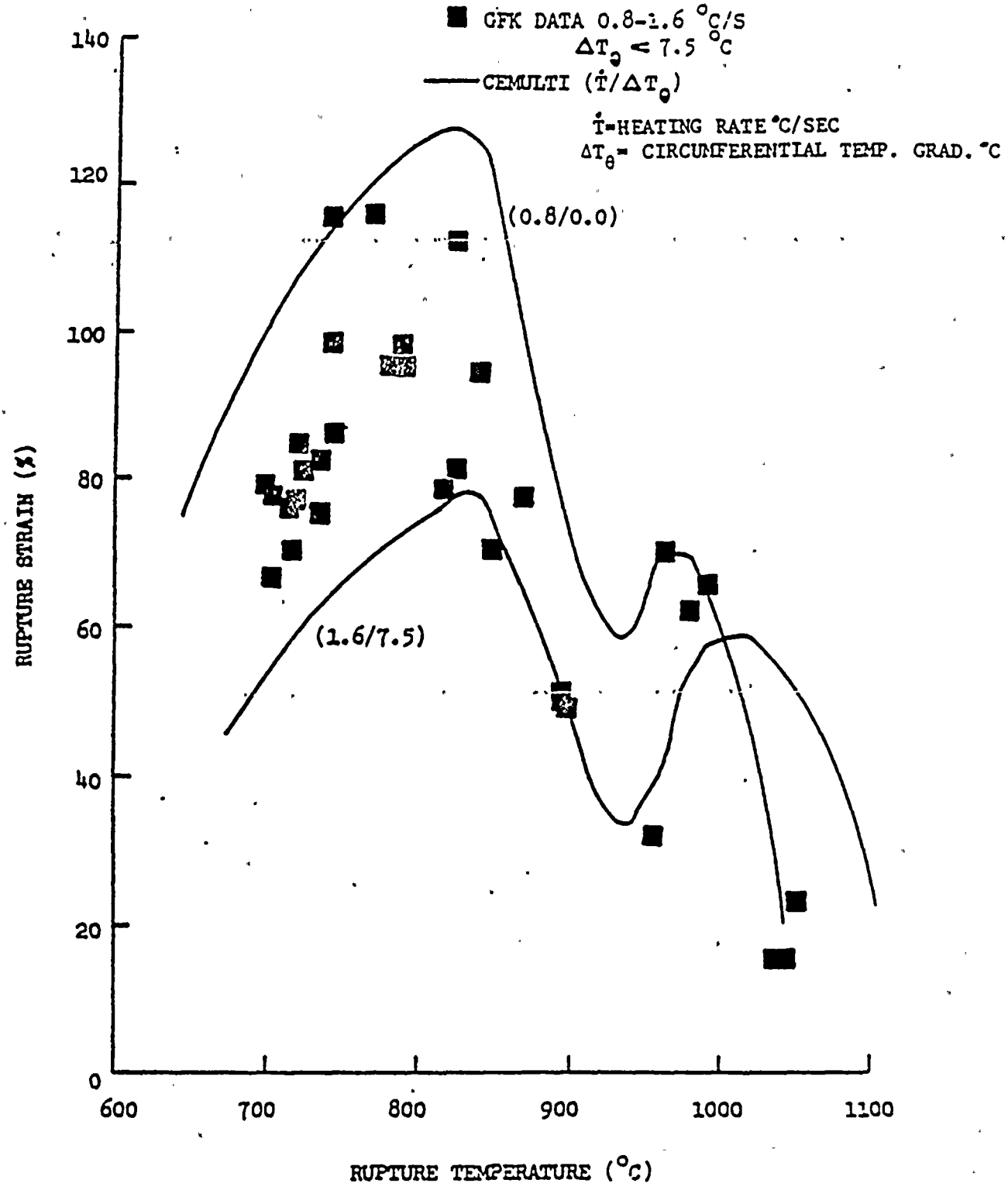

Figure 2.16-3
Comparison of CEMULTI to GFK Data
Rupture Strain Vs. Rupture Temperature
Heating Rate ≈ 10 °C/Sec

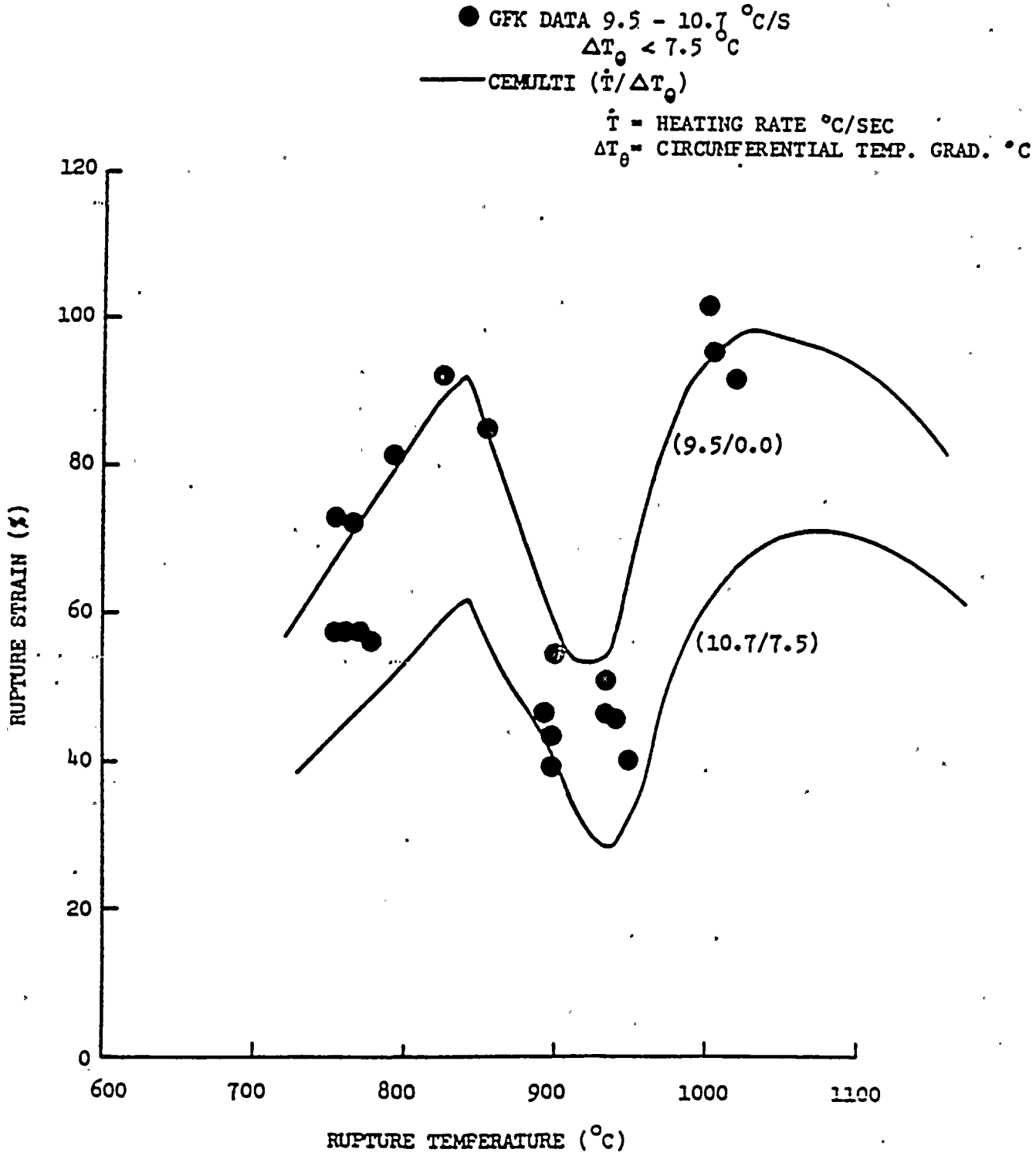

Figure 2.16-4
Comparison of CEMULTI to GFK Data
Rupture Strain Vs. Rupture Temperature
Heating Rate ≈ 30 °C/Sec

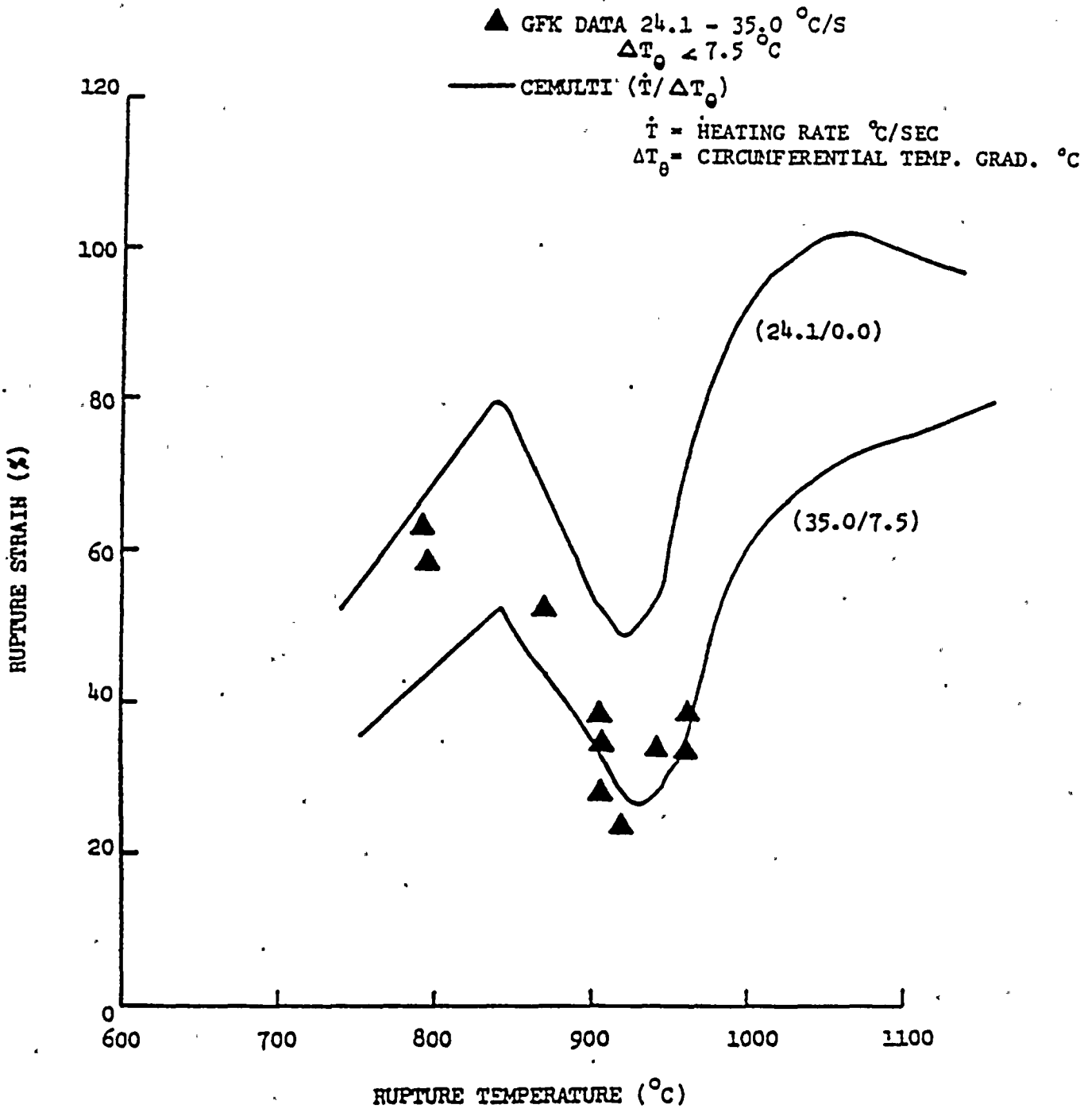

Figure 2.16-5
Comparison of CEMULTI to GFK Data
Rupture Temperature Vs. Differential Pressure

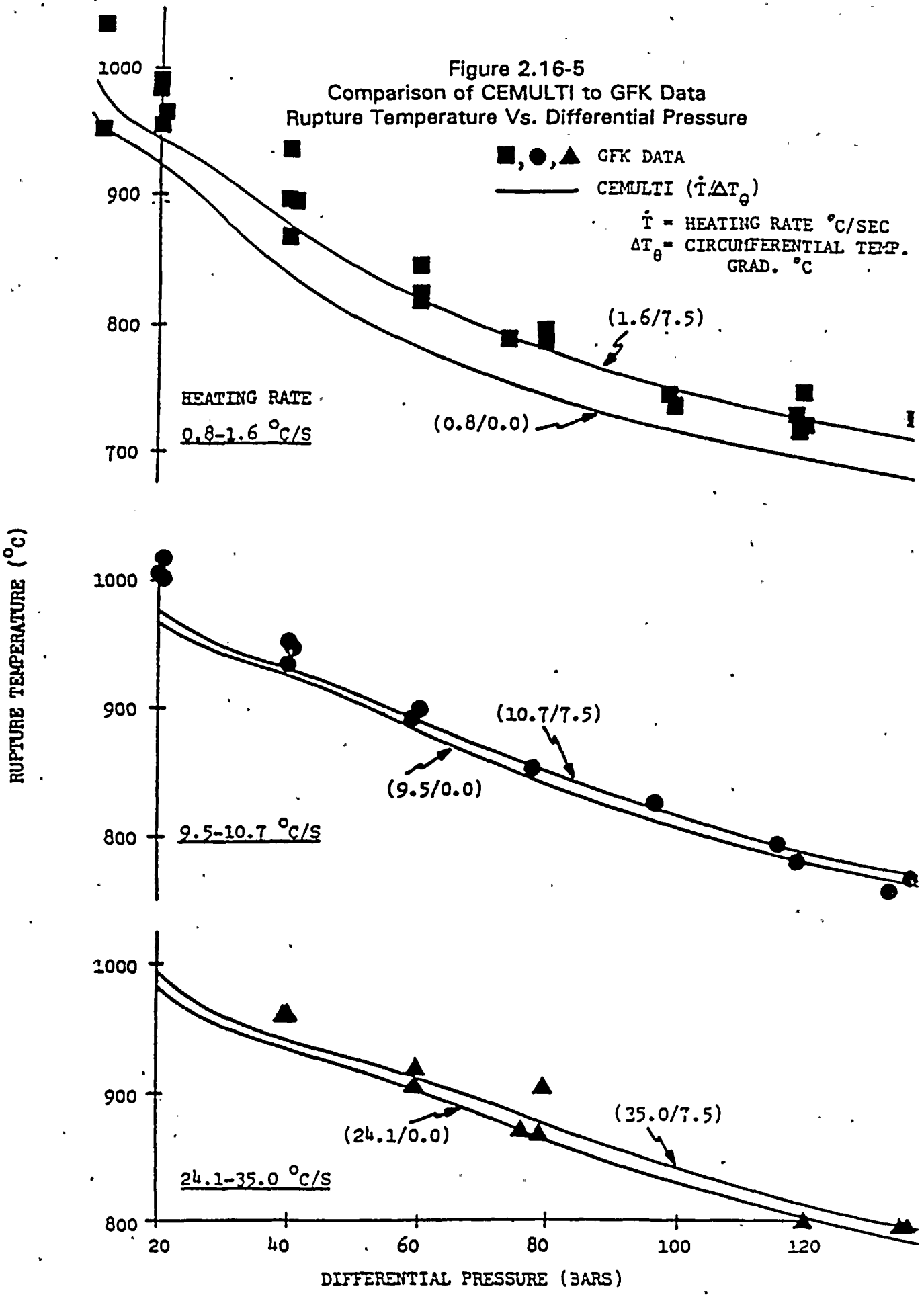

Figure 2.16-6
CEMULTI Comparison to C-E SREPT Burst Data

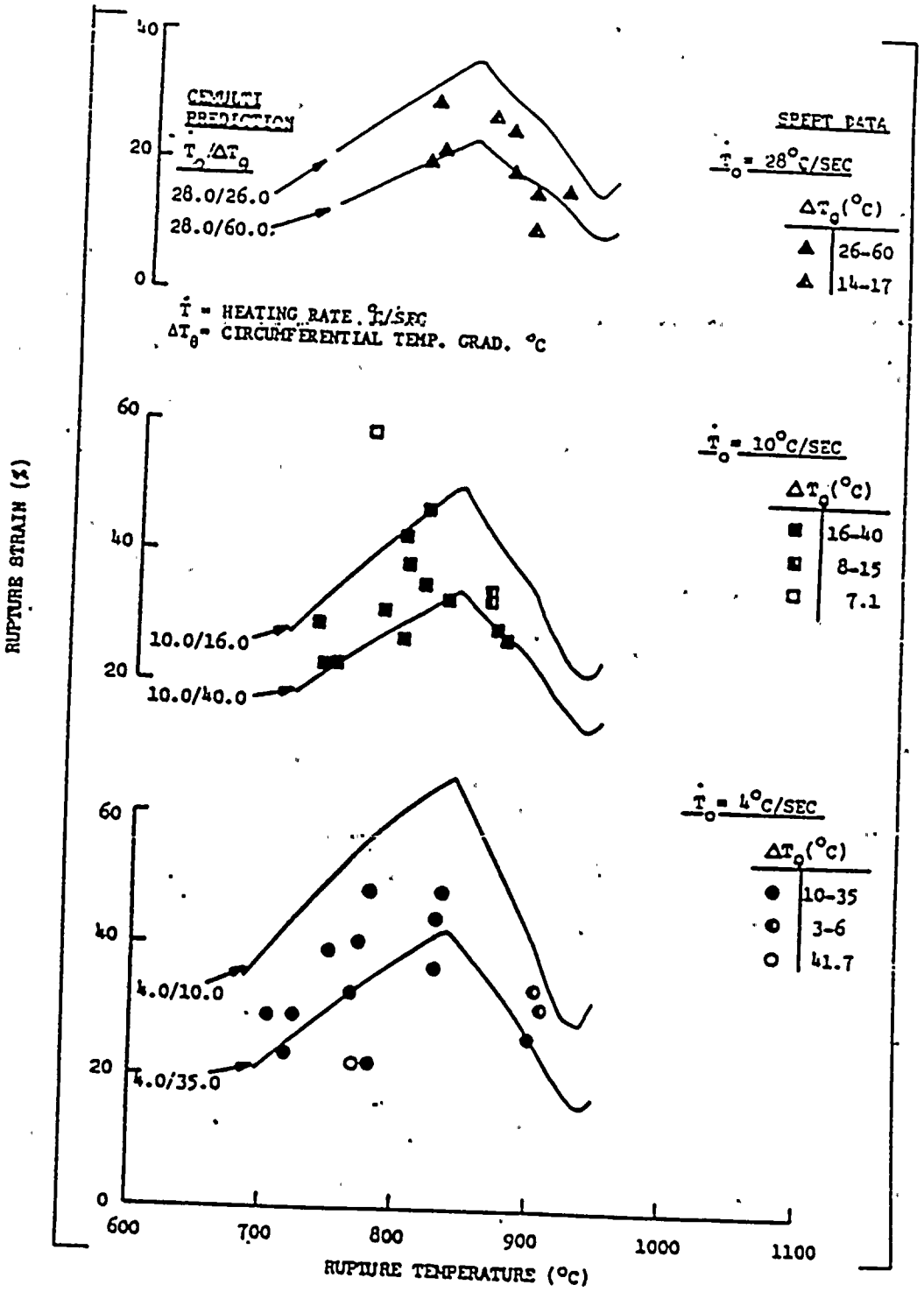

Figure 2.16-7
C-E SREPT Burst Test #19

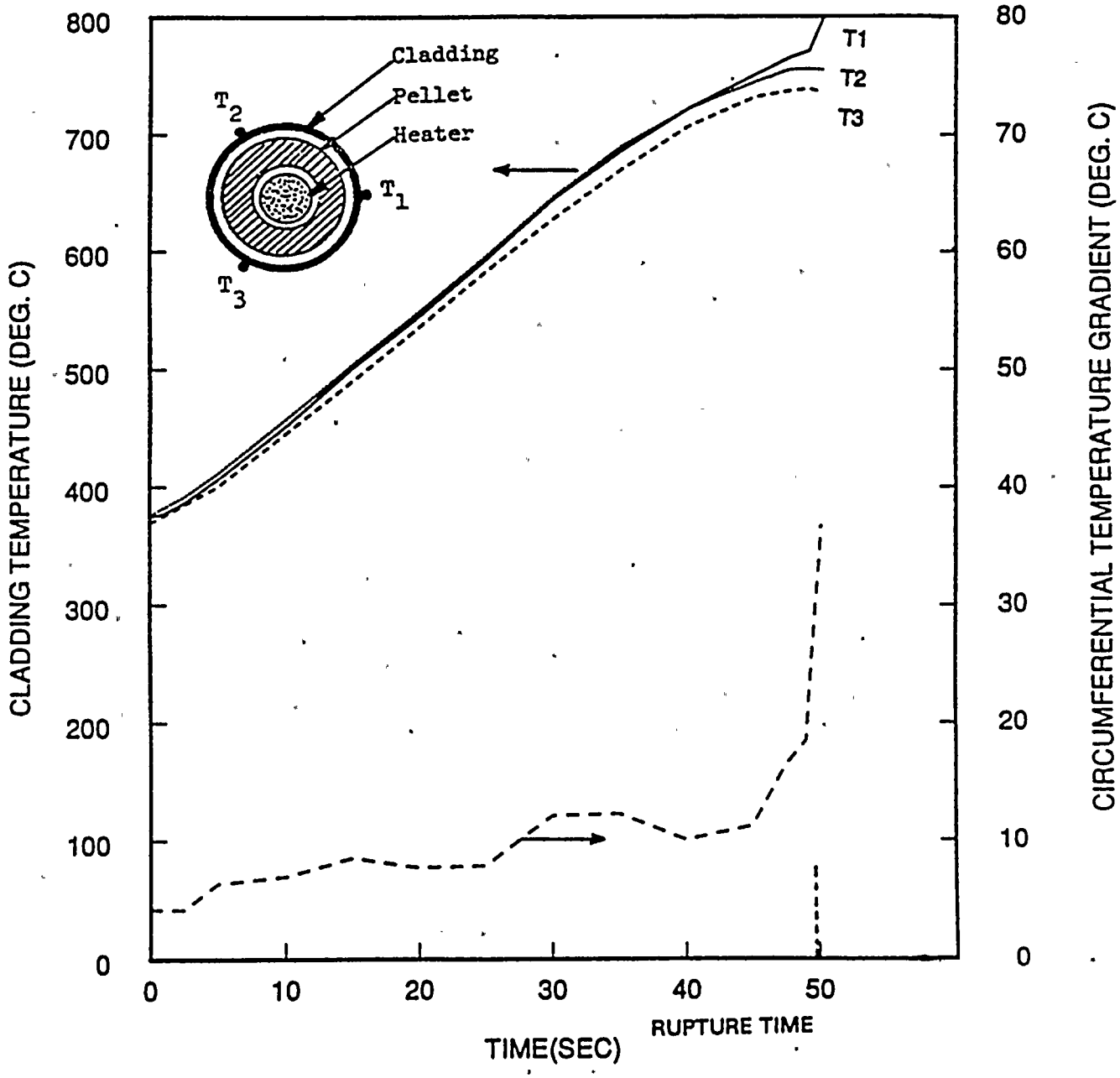

Figure 2.16-8
C-E SREPT Burst Test #20

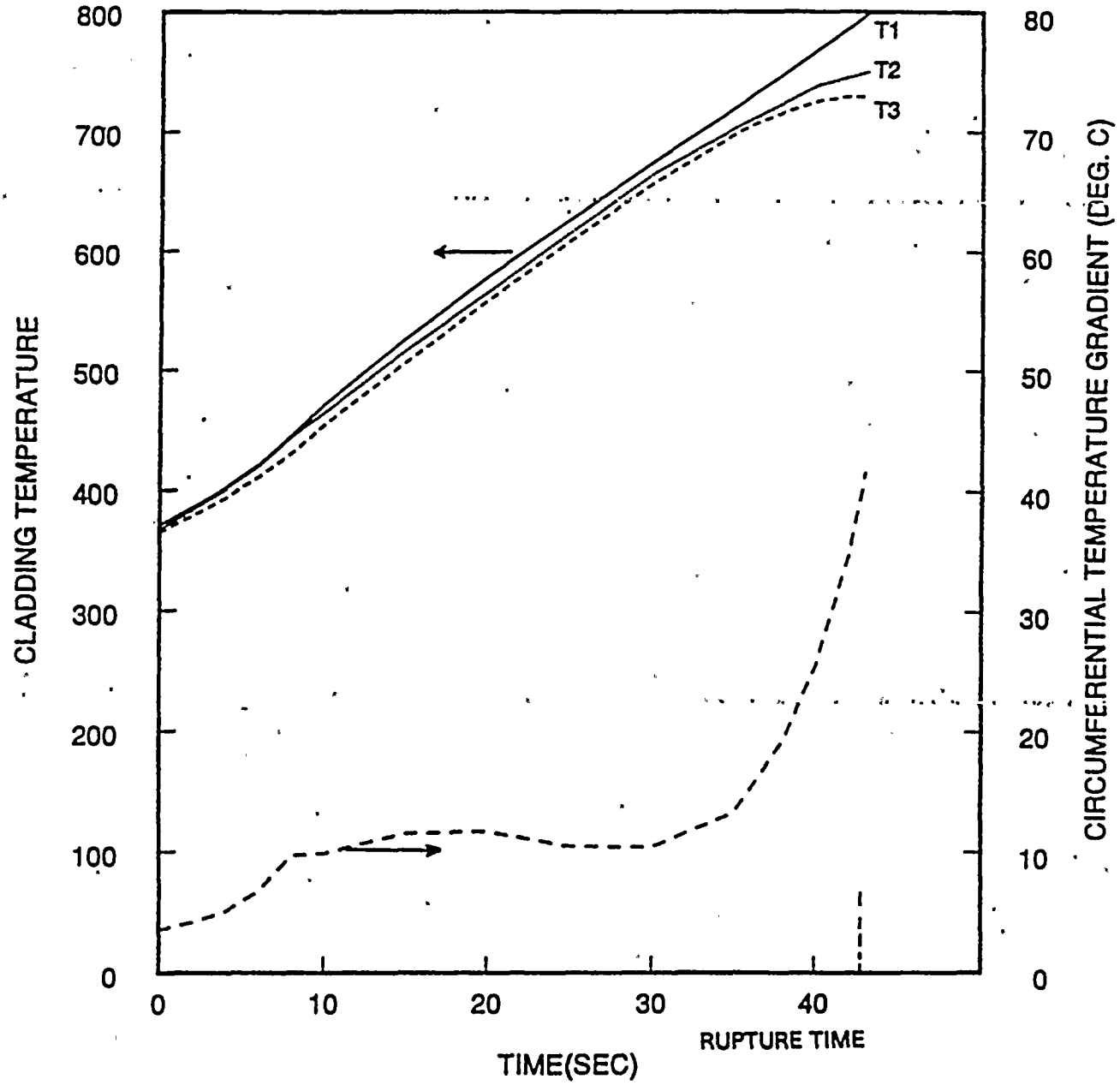

Figure 2.16-9
C-E SREPT Burst Test #31

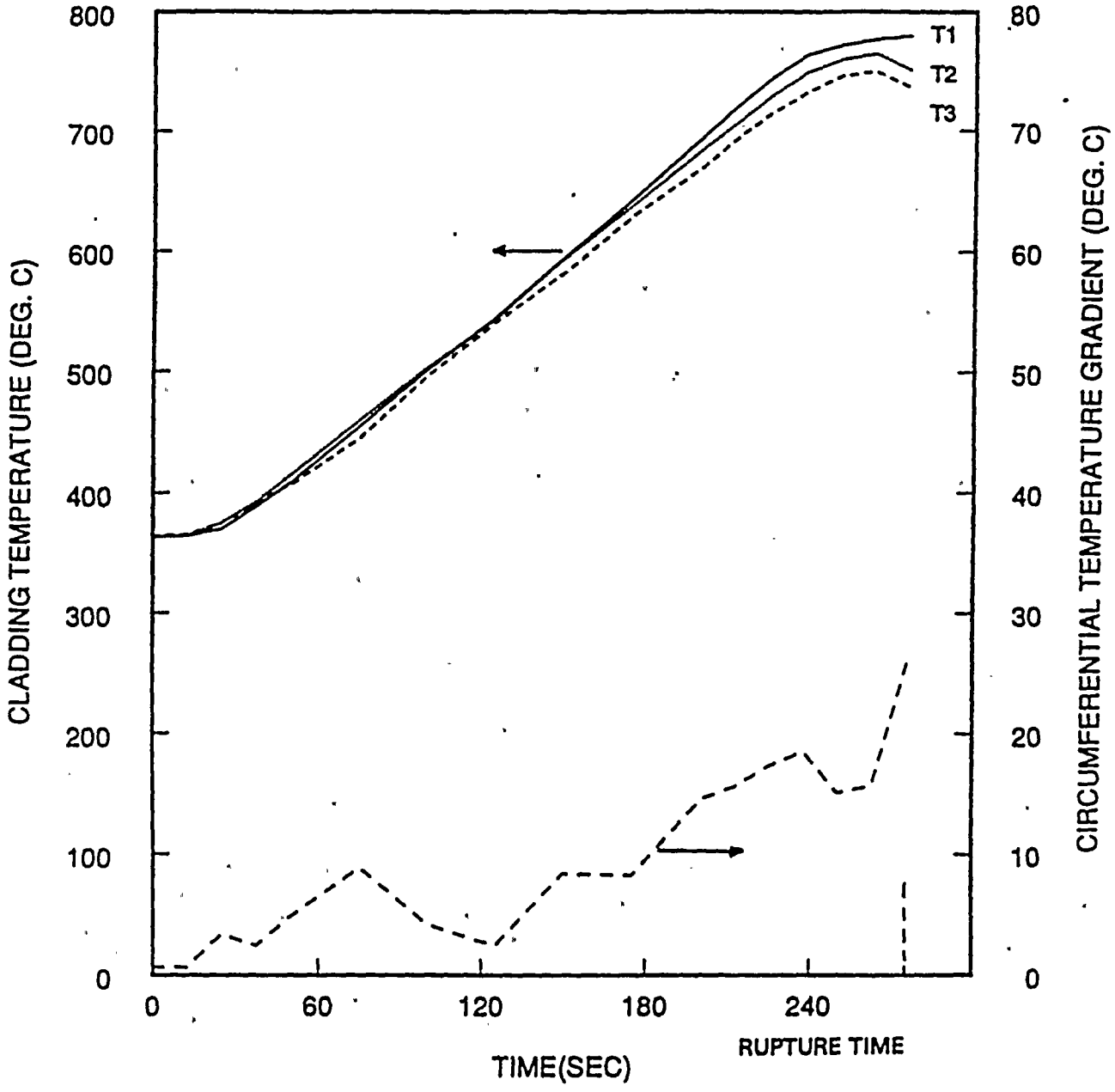

Figure 2.16-10
C-E SREPT Burst Test #49

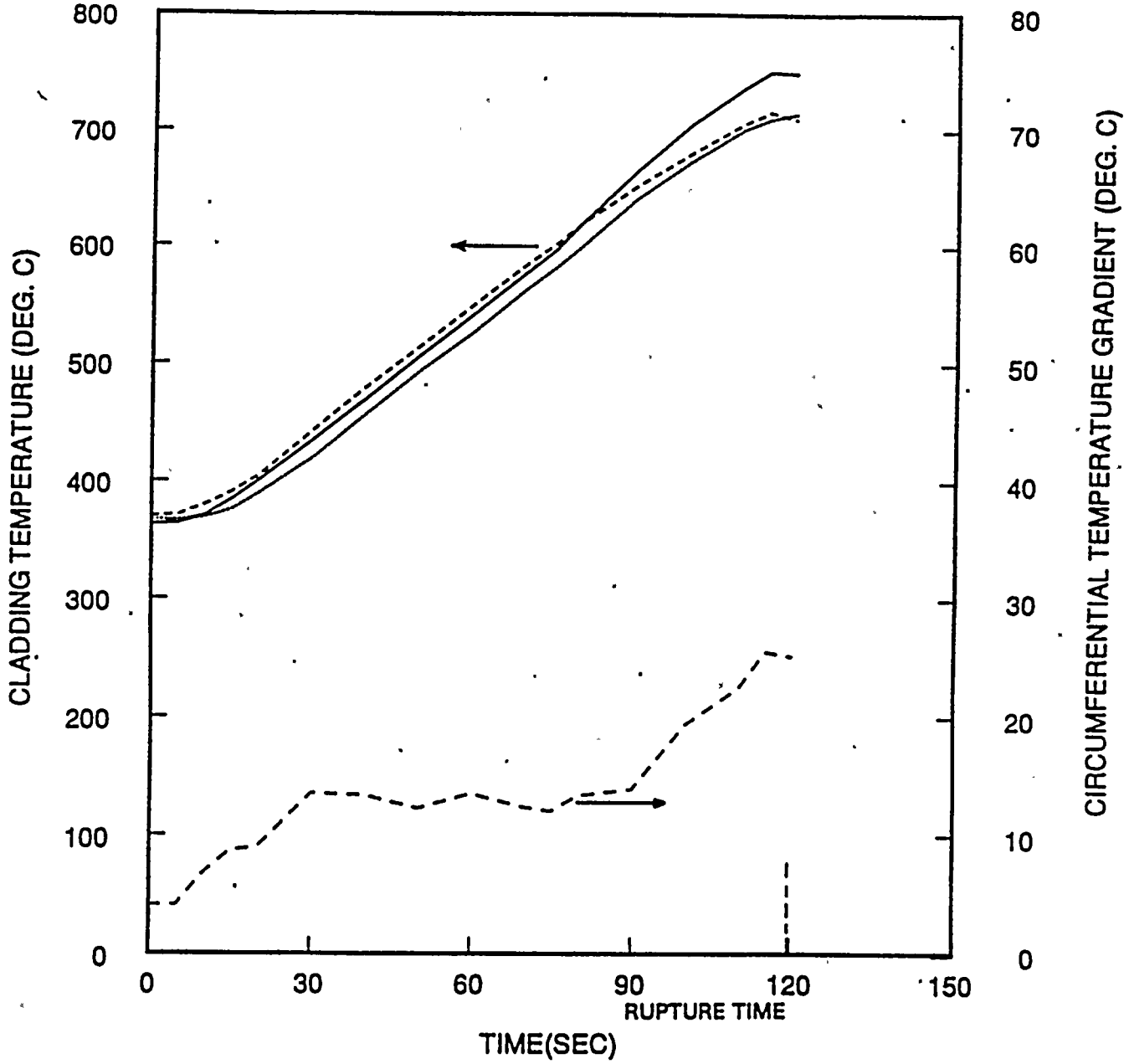

Figure 2.16-11
C-E SREPT Burst Test #50